HSulf-1 Inhibits Angiogenesis and Tumorigenesis *In vivo*

Keishi Narita,[1] Julie Staub,[1] Jeremy Chien,[1] Kristy Meyer,[2] Maret Bauer,[2] Andreas Friedl,[2] Sundaram Ramakrishnan,[3] and Viji Shridhar[1]

[1]Department of Experimental Pathology, Mayo Clinic Cancer Center, Rochester, Minnesota; [2]Department of Pathology and Laboratory Medicine, University of Wisconsin, Madison, Wisconsin; and [3]Department of Pharmacology, University of Minnesota, Minneapolis, Minnesota

Abstract

We previously identified HSulf-1 as a down-regulated gene in several tumor types including ovarian, breast, and hepatocellular carcinomas. Loss of HSulf-1, which selectively removes 6-*O*-sulfate from heparan sulfate, up-regulates heparin-binding growth factor signaling and confers resistance to chemotherapy-induced apoptosis. Here we report that HSulf-1 expression in MDA-MB-468 breast carcinoma clonal lines leads to reduced proliferation *in vitro* and reduced tumor burden in athymic nude mice *in vivo*. Additionally, xenografts derived from HSulf-1–expressing stable clones of carcinoma cells showed reduced vessel density, marked necrosis, and apoptosis, indicative of inhibition of angiogenesis. Consistent with this observation, HSulf-1–expressing clonal lines showed reduced staining with the endothelial marker CD31 in Matrigel plug assay, indicating that HSulf-1 expression inhibits angiogenesis. More importantly, HSulf-1 expression in the xenografts was associated with a reduced ability of vascular endothelial cell heparan sulfate to participate in a complex with fibroblast growth factor 2 (FGF-2) and its receptor tyrosine kinase FGF receptor 1c. *In vitro*, short hairpin RNA–mediated down-regulation of HSulf-1 in human umbilical vein endothelial cells (HUVEC) resulted in an increased proliferation mediated by heparan sulfate–dependent FGF-2, hepatocyte growth factor, and vascular endothelial growth factor 165 ($VEGF_{165}$) but not by heparan sulfate–independent $VEGF_{121}$. HSulf-1 down-regulation also enhanced downstream signaling through the extracellular signal–regulated kinase pathway compared with untreated cells. Consistent with the role of heparan sulfate glycosaminoglycan sulfation in VEGF-mediated signaling, treatment of HUVEC cells with chlorate, which inhibits heparan sulfate glycosaminoglycan sulfation and therefore mimics HSulf-1 overexpression, led to an attenuated VEGF-mediated signaling. Collectively, these observations provide the first evidence of a novel mechanism by which HSulf-1 modulates the function of heparan sulfate binding $VEGF_{165}$ in proliferation and angiogenesis. (Cancer Res 2006; 66(12): 6025-32)

Introduction

Tumor angiogenesis is characterized by the formation of new irregular blood vessels from a preexisting vascular network. This abnormal angiogenesis is required for the growth, survival, and metastasis of most solid tumors (1, 2). Vascular endothelial growth factor (VEGF) is one of the most important proangiogenic factors, which acts as a mitogen for vascular endothelial cells *in vitro* and as an angiogenic factor *in vivo* (3). It is overexpressed in various human cancers (4–7). There are four alternatively spliced forms of VEGF coding for 121-, 165-, 189-, and 206-amino-acid polypeptides. $VEGF_{165}$, unlike the smallest isoform, $VEGF_{121}$, has a heparin-binding domain encoded by the exon 7. In vascular endothelial cells, heparan sulfate proteoglycans (HSPG), important structural components of extracellular matrix, are required for efficient binding of $VEGF_{165}$ to its cognate receptors (8, 9). Using an ELISA, Ono et al. (10) showed that whereas native heparin interacted with $VEGF_{165}$, *N*-desulfated, *N*-acetylated, and 6-*O* desulfated heparin did not, implicating a crucial role for the sulfation status of heparan sulfate in $VEGF_{165}$ signaling. Interestingly, the 6-*O* sulfate domain plays a similarly crucial role in signaling of the potent proangiogenic factor fibroblast growth factor (FGF-2; ref. 11).

Our previous *in vitro* study showed that a frequently down-regulated gene, HSulf-1, in ovarian and breast cancer cell lines modulates signaling of a variety of heparin-binding growth factors, cell proliferation, chemosensitivity, and the invasive phenotype of cancer cells (12–14). In the present study, we extend our previous observations to show that HSulf-1 inhibits both tumor growth and tumor angiogenesis *in vivo*. This inhibition of angiogenesis is, at least in part, due to a significantly reduced ability of vascular heparan sulfate to support a stable complex with FGF-2 and FGF receptor 1c (FGFR1c) in HSulf-1 xenografts. Consistent with this notion, we show that short hairpin RNA (shRNA)–mediated down-regulation of HSulf-1 modulates the $VEGF_{165}$-induced angiogenic response of normal endothelial cells. These data provide evidence that HSulf-1 plays a key role in regulating not only tumor growth but also angiogenesis.

Materials and Methods

Materials. Growth factor–reduced Matrigel and antimouse CD31 monoclonal antibody (clone MEC13.3) were obtained from BD Biosciences (San Jose, CA). *In situ* Cell Death Detection Kit was from Roche Applied Science (Indianapolis, IN). Phycoerythrin-conjugated antimouse CD31 antibody was obtained from PharMingen (San Jose, CA). Human recombinant $VEGF_{165}$, $VEGF_{121}$, FGF-2, hepatocyte growth factor, and heparin-binding epidermal growth factor (EGF)–like growth factor ligands were purchased from R&D Systems (Minneapolis, MN). Antibodies against total extracellular signal–regulated kinase (ERK) 1/2, phospho-ERK1/2 (Thr^{202}/Tyr^{204}), total kinase-insert-domain-containing receptor (KDR), and phospho-KDR (Tyr^{1175}) were from Cell Signaling Technology (Beverly, MA). pSuper.retro.puro was from OligoEngine (Seattle, WA). Monoclonal anti–heparan sulfate (10E4 epitope) was from Seikagaku (Tokyo, Japan). Monoclonal antitubulin antibody and polybrene were from Sigma (St. Louis, MO). Polyclonal anti-myc antibody was from Santa Cruz Biotechnology (Santa Cruz, CA). [methyl-^{3}H]Thymidine (20 Ci/mmol) was from Perkin-Elmer (Wellesley, MA). Horseradish peroxidase–conjugated rabbit

Requests for reprints: Viji Shridhar, Mayo College of Medicine, 200 First Street Southwest, Rochester, MN 55905. Phone: 507-266-2775; Fax: 507-266-5193; E-mail: shridhar.vijayalakshmi@mayo.edu and Andreas Friedl. E-mail: afriedl@facstaff.wisc.edu.

doi:10.1158/0008-5472.CAN-05-3582

immunoglobulin G and enhanced chemiluminescence and Western blotting detection reagents were from Amersham Biosciences (Piscataway, NJ).

Cell culture. The breast cancer cell line MDA-MB-468 (hereafter referred to as MDA468) and the ovarian cancer cell line SKOV3 were obtained from American Type Culture Collection (Manassas, VA). These cells were cultured in DMEM containing 10% fetal bovine serum (FBS), 1% penicillin/streptomycin, and 0.1% amphotericin B. Human umbilical vein endothelial cells (HUVEC) and endothelial cell basal medium were obtained from Cambrex (Walkersville, MD). HUVECs were cultured in endothelial cell basal medium supplemented with 2% FBS, 0.4% bovine brain extract, 0.1% human EGF, 0.1% hydrocortisone, and 0.1% GA-1000.

Isolation of cancer cell lines stably expressing HSulf-1 and *in vitro* cell proliferation assay. Isolation of MDA468 stable clones expressing HSulf-1 and the verification by RT-PCR and sulfatase assay and *in vitro* cell proliferation assay were carried out as previously described (12).

Tumor xenograft experiments. All mice were handled according to the Guide for the Care and Use of Laboratory Animals. Mouse studies were carried out following procedures approved by the Institutional Animal Care and Use Committee at the Mayo Clinic College of Medicine. Female athymic nude mice (NCr *nu/nu*; Animal Production Area, National Cancer institute-Frederick Cancer Research and Development Center, Frederick, MD), 5 to 6 weeks old, were used for this study. For measurement of tumor growth *in vivo*, MDA468 clones (10^7 cells per mouse) were mixed with Matrigel and injected s.c. in the left flanks of mice, 10 mice per clone. Tumor volume was calculated weekly by caliper measurements using the following formula: tumor volume (mm^3) = $(W \times H \times D) / 2$, where W is width, H is height, and D is depth in millimeters. Tumor xenografts were recovered from mice, fixed in formalin, and embedded in paraffin. Tissue sections were used for detection of necrotic cells (areas) by H&E staining or with Masson's trichrome stain for visualization of collagen or apoptotic cells by TUNEL staining using the *In situ* Cell Death Detection Kit.

Microvessel density analysis and Matrigel plug assays. For measurement of microvessel density, frozen sections from the xenograft tissues were fixed in acetone and allowed to air-dry. After rinsing and blocking, the sections were incubated with anti-mouse CD31 monoclonal antibody (clone MEC13.3) at 10 μg/mL for 1 hour, followed by Alexa-568-conjugated secondary goat anti-rat antibody at 1:400 dilution, and 4′,6-diamidino-2-phenylindole (DAPI) counterstain. Sixteen-bit grayscale epifluorescence images were acquired with a SPOT-RT Slider cooled CCD camera (Diagnostic Instruments, Sterling Heights, MI). The images were analyzed in ImageJ (NIH, public domain), yielding vessel count per image field and total vessel area.

To investigate changes in microvessel architecture, MDA468 and SKOV3 clones (10^6 cells) mixed with Matrigel were injected s.c. into nude mice and the Matrigel plugs were recovered 1 week postinjection. Matrigel plugs were snap frozen in liquid nitrogen in the presence of optimum cutting temperature compound and sectioned. Frozen Matrigel sections were fixed in cold acetone and immunostained with phycoerythrin-conjugated anti-CD31 antibody for microvessel density measurement as previously described (15).

Glycosaminoglycan receptor complex binding assay *in situ*. The ability of tumor xenograft tissue heparan sulfate to form a ternary complex with FGF-2 ligand and FGFR1c was assayed with an *in situ* glycosaminoglycan receptor complex reconstitution assay as previously described (16, 17). Briefly, tumor cryosections were incubated with FGF-2 (30 nmol/L) and FGFR1c-alkaline phosphatase (FR1c-AP; 100 nmol/L), a fusion protein consisting of the extracellular domain of FGFR1c and placental alkaline phosphatase. Negative controls included heparan sulfate degradation with heparitinase or omission of FGF-2. Tumor vessels were identified by dual labeling with rat anti-CD31 antibody as described above. Bound FR1c-AP and anti-CD31 antibody were visualized with Alexa-488- and Alexa-568-conjugated secondary antibodies, respectively. The viable tumor area was imaged with an Olympus BX50 microscope equipped for epifluorescence and fitted with a cooled charge-coupled device camera (DP70, Olympus, Melville, NY). To analyze FR1c-AP fluorescence intensity in blood vessels, the CD31-positive areas were selected using the "magic wand" tool within the Photoshop program (Adobe, San Jose, CA). A mask, which excluded the CD31-negative area, was superimposed on the corresponding FR1c-AP image. The average FR1c-AP fluorescence intensity within the vascular areas was measured with ImageJ software.

Construction of shRNA plasmids and retroviral infection of HUVECs. For down-regulation of HSulf-1 expression in HUVECs, a retrovirus-mediated shRNA technique was used. The candidate siRNA sequences targeting HSulf-1 mRNA were generated using the Ambion server[4] and screened based on previously described criteria (18) to select two sequences, targeting positions 802-820 (T1) and 1,492-1,510 (T2) of HSulf-1 mRNA. The oligonucleotide pairs used were T1F (5′-GATCCCCGTATGTGCACAATCACAATTTCAAGAGAATTGTGATTGTGCACATACTTTTTGGAAA-3′), T1R (5′-ACGTTTTCCAAAAAGTATGTGCACAATCACAATTCTCTTGAAATTGTGATTGTGCACATACGGG-3′), T2F (5′-GATCCCCGGGGAAATCCATGCCATATTTCAAGAGAAGATGGCATGGATTTCCCCTTTTTAA-3′), and T2R (5′-AGCTTAAAAAGGGGAAATCCATGCCATCTTCTCTTGAAATATGGCATGGATTTCCCCGGG-3′). The underlined sequences in each forward primer indicate the 19-nucleotide stretches that form the hairpin. The oligonucleotide pairs were annealed and ligated into the *Bgl*II-*Hin*dIII sites of pSUPER.retro.puro vector following the protocol of the manufacturer. The resulting two plasmid constructs were combined (designated as pSR-HSulf-1), packaged into infectious retrovirus in HEK293T cells expressing gag, pol, and env proteins. For control experiments, empty pSUPER.retro vector (designated as pSR alone) was packaged into retrovirus. The conditioned medium containing pSUPER.retro viral particles was filtered through a 0.45-μm filter and stored at −80°C. For transfection, HUVECs plated on the day before were incubated for 48 hours with 1:1 mixture of the viral supernatants and fresh culture medium in the presence of 4 μg/mL polybrene. The efficacy of shRNA was evaluated by RT-PCR, sulfatase assay (12), and immunostaining for 10E4 epitope (19) as described.

[^{3}H]Thymidine incorporation assay. [^{3}H]Thymidine incorporation assay was carried out as described elsewhere (20) with some modification. Briefly, HUVECs were seeded on 24-well plates at 20,000 per well, incubated overnight, and transfected with the above retroviral constructs for 24 hours. The transfected cells were incubated in serum-free medium containing 0.5 μCi [^{3}H]thymidine and various growth factors to be tested for 24 hours. After washing with PBS, the incubation was stopped with 5% ice-cold trichloroacetic acid. The samples were washed with 70% ethanol, air-dried, dissolved in 1% SDS, and the radioactivity was quantified by scintillation counter.

Treatment of HUVECs with VEGF and analysis of ERK and KDR phosphorylation by immunoblotting. HUVECs transfected with the retroviral constructs as described above were serum starved overnight and then treated with $VEGF_{165}$ (5 ng/mL) or $VEGF_{121}$ (20 ng/mL) for various times at 37°C. The cells were quickly rinsed with ice-cold PBS and lysed at 4°C in SDS sample loading buffer. The resulting protein samples were separated on SDS-PAGE, transferred to polyvinylidene difluoride (PVDF) membrane, and analyzed by immunoblotting as previously described (12). The antibodies used for immunoblotting and their dilutions were as follows: phospho-ERK (1:500), total ERK (1:500), phospho-KDR (1:250), total KDR (1:250), and tubulin (1:1,000).

Chlorate treatment of HUVECs following stimulation with VEGF. HUVECs were seeded on six-well plates at an initial density of 100,000 per well and incubated 48 hours in sulfate-free DMEM containing 15 mmol/L sodium chlorate. The cells were serum starved overnight in sulfate-free DMEM and then treated with 5 ng/mL $VEGF_{165}$ for 0, 15, and 60 minutes. Lysates were analyzed by Western blotting for activation of ERK as previously described. Cells not treated with chlorate served as controls.

Statistical analysis. All values are expressed as mean ± SE. Differences between two groups were compared using an unpaired two-tailed t test. When comparing multiple groups, one-way ANOVA followed by Newman-Keul's test was used. Results were considered significant at $P < 0.05$.

[4] http://www.ambion.com.

Results

HSulf-1 reexpression in MDA468 breast carcinoma causes reduced growth rate and enhanced cell death. To investigate the role of HSulf-1 in tumor progression, we established multiple stable clones expressing HSulf-1 using a poorly differentiated breast cancer cell line, MDA468, which lacks endogenous HSulf-1 expression. The expression of HSulf-1 was confirmed by RT-PCR and sulfatase assay (Fig. 1*A* and *B*). As reported previously with SKOV3 and OV207 ovarian cancer cell lines (12), expression of HSulf-1 in MDA468 resulted in reduced cell proliferation (Fig. 1*C*). To further examine the effect of HSulf-1 expression in tumorigenesis *in vivo*, we injected both the vector-transfected and HSulf-1–expressing MDA468 stable clones s.c. into athymic nude mice and monitored tumor volume over a 27-week period (Fig. 2*A*). The presence of HSulf-1 in MDA468 clonal lines 4 and 5 resulted in a dramatic reduction in tumor volume compared with the vector-transfected clone. During the initial 2 weeks postinjection, no significant differences in tumor size were observed among the different groups. However, the mice injected with HSulf-1 clonal lines 4 and 5 began to show significant inhibition in tumor growth after 12 and 3 weeks postinjection, respectively, whereas the xenografts from the vector-transfected control showed continued increases in tumor mass. At 27 weeks postinjection, the mean tumor sizes of HSulf-1 clones 4 and 5 were 306 ± 145 and 213 ± 63 mm^3, respectively, whereas that of vector derived xenografts was 1,510 ± 611 mm^3. Thus, the vector-derived xenografts showed a 5-fold increase in tumor volume compared with xenografts derived from HSulf-1 clonal lines 4 and 5. The xenografts derived from the vector-transfected clone were large, round, and highly vascularized whereas those of HSulf-1 clones were small, collapsed, and pale in appearance (Fig. 2*A, inset*). These data indicate that the growth of HSulf-1 clones *in vivo* was significantly reduced compared with the vector-transfected clone.

To investigate if the tumor inhibitory effect of HSulf-1 is associated with induction of cell death, a histopathologic examination was done. H&E staining of tumor xenografts recovered at 27 weeks postinjection (Fig. 2*B*) showed that tumor xenografts of HSulf-1 clones were highly necrotic with only 30% of the total area as H&E positive, compared with the more viable vector clone, with ~75% of the total area as H&E positive (Fig. 2*B*).

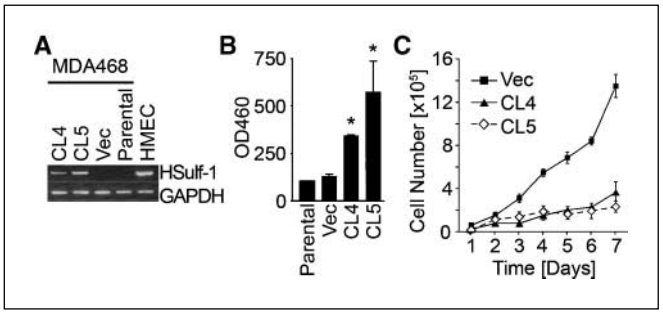

Figure 1. Isolation and characterization of MDA468 clones stably expressing HSulf-1. *A,* RT-PCR of HSulf-1–transfected clone 4 (*CL4*) and clone 5 (*CL5*), vector-transfected clone (*Vec*), and parental MDA468. *HMEC,* normal human mammary epithelial cells. *B,* HSulf-1 clones exhibit higher sulfatase activity. Cell extracts from the stable clones were assayed for sulfatase activity using 4-MUS in the presence of 10 mmol/L estrone 3-*O*-sulfamate, an inhibitor of endogenous steroid sulfatase, as described (12). *, $P < 0.05$, versus vector-transfected clone. *C,* HSulf-1 expression reduces cell proliferation. The cells were plated at 100,000 per dish in triplicate and examined daily after trypan blue staining to determine the number of viable cells per plate.

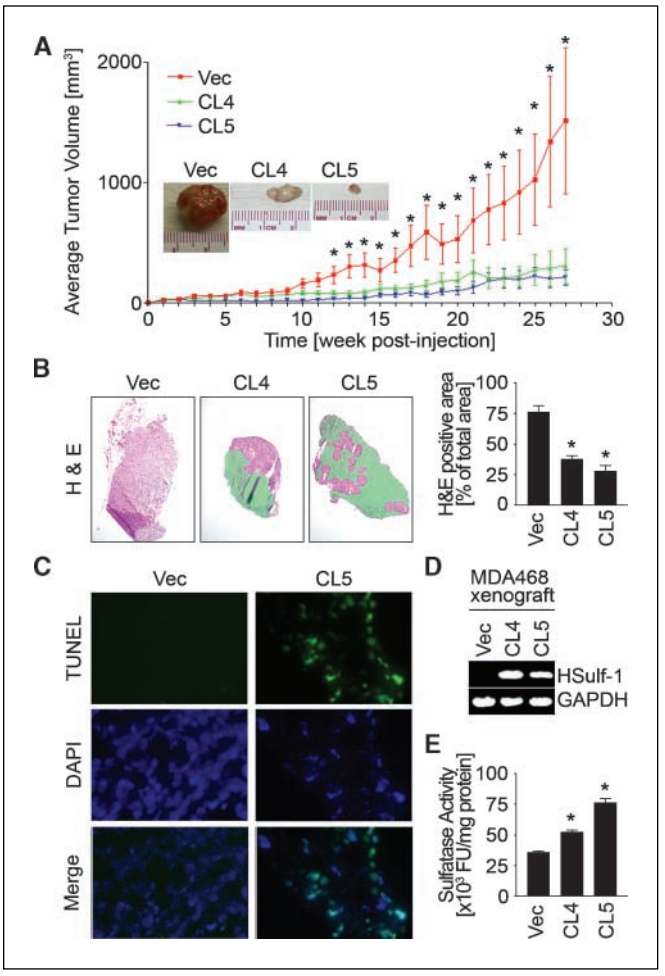

Figure 2. Reduced proliferation and enhanced cell death of MDA468 HSulf-1 clones injected in mice. *A,* growth curve of MDA468 clones in athymic nude mice. MDA468 clones (10^7 cells per mouse) were mixed with Matrigel and injected s.c. the in left flanks of female, 4- to 5-week-old athymic *nu/nu* mice ($n = 10$). *, $P < 0.05$, versus HSulf-1 clones. *Inset,* representative images of tumor xenografts from each clone. *B,* detection of necrosis in tumor xenografts of MDA468 clones. *Green,* necrotic regions identified by H&E staining. Images were taken with 20× objective. *Right,* quantification of the viable, H&E-positive area by image analysis. Six different xenografts for each clone were analyzed. *, $P < 0.05$, versus vector-transfected control. *C,* detection of apoptotic cells by TUNEL staining (*green*). The samples were costained with DAPI (*blue*) to identify the nuclei. *D,* persistent expression of HSulf-1 in clonal xenografts was confirmed by RT-PCR. *E,* HSulf-1 xenografts exhibit higher sulfatase activity. Sulfatase activity was determined as described in Materials and Methods.

Similarly, the TUNEL assay showed that apoptosis was induced in the HSulf-1 tumor xenografts but not in the vector-derived xenografts (Fig. 2*C*). These data indicate that the reduced tumor growth of MDA468 HSulf-1 clones *in vivo* could be due to enhanced necrosis and apoptosis. Persistent expression of HSulf-1 in clonal xenografts was confirmed by both RT-PCR (Fig. 2*D*) and sulfatase activity assay (Fig. 2*E*).

Reduced tumor growth of HSulf-1–expressing MDA468 clones *in vivo* is associated with inhibition of tumor angiogenesis. Most solid tumors, including breast and ovarian cancers, require new blood vessel formation to grow beyond a few millimeters in diameter (21). Because HSulf-1 catalyzes the 6-*O* desulfation of HSPGs and should therefore affect the activity of heparin-binding angiogenic factors including $VEGF_{165}$, we postulated that MDA468 HSulf-1 clones might induce less tumor angiogenesis. To test this hypothesis, we did Matrigel plug assays

to determine the changes in microvessel architecture in detail when the xenograft tumor volumes of both HSulf-1 expressors and nonexpressors were similar (i.e., 1 week postinjection). The Matrigel plugs containing the vector-transfected clone 5 showed a high degree of microvessel density with elongated, complex morphology. By contrast, the plugs of HSulf-1 clones showed a significantly lesser number of blood vessels with poorly developed vascular structures (Fig. 3*A*). To evaluate the level of microvessel density in more detail, the fluorescent images of the anti-CD31-stained tumor sections were digitally recorded and used for computer-assisted image analysis (Fig. 3*B*). This analysis indicated that the HSulf-1 clones had significantly reduced tumor angiogenesis, showing >60% reduction in vessel ends, vessel nodes, and total vessel length. The same experiment done using SKOV3 ovarian cancer cells showed that HSulf-1 expression was associated with reduced angiogenesis (Fig. 3*C*). The SKOV3 HSulf-1 clonal lines 7 and 8 had >70% reduction in angiogenic indices. These data indicated that HSulf-1 inhibits tumor angiogenesis in the nude mouse model. Similarly, when we investigated the levels of tumor-induced microvessel density in tumor xenografts, the microvessel density was significantly reduced in xenografts of HSulf-1 clones compared with cells transfected with empty vector (Fig. 3*D*).

Analysis of FGF-2/heparan sulfate/FR1c-AP complex formation. One possible explanation for reduced angiogenesis in HSulf-1–expressing tumors would be the removal of 6-*O* sulfate from vessel endothelial cell heparan sulfate by the secreted enzyme. The modified heparan sulfate would be expected to possess an inferior ability to activate proangiogenic growth factors (e.g., supporting a ternary complex with FGF-2 and FGFR1c). This hypothesis was tested with the glycosaminoglycan receptor complex assay, which measures binding of FR1c-AP fusion protein to frozen sections of tumors (source of heparan sulfate) in the presence of FGF-2 (16). Tumor vessel endothelial cells were identified by double staining with an antibody to CD31 (Fig. 4*A* and *B*). MDA468 clone 4 and clone 5 generated xenografts showed a trend towards reduced binding compared with vector-generated xenografts when total tissue FR1c-AP binding signal was evaluated, but the difference did not reach statistical significance (data not shown). However, FR1c-AP binding to endothelial cell heparan sulfate was significantly ($P < 0.001$) reduced in HSulf-1-transfected tumors (both clones 4 and 5) compared with vector transfected controls (Fig. 4*C*). Moreover, the endothelial FR1c-AP binding signal was lower in clone 5 tumors than in clone 4 tumors ($P < 0.001$), suggesting an HSulf-1 dose effect (Fig. 4*C*).

No difference in stromal content or architecture was detected between tumors formed by vector control, clone 4, or clone 5 cells on Masson trichrome–stained paraffin sections (Fig. 4*D*).

siRNA-mediated down-regulation of HSulf-1 expression in HUVEC. Because the VEGF produced by epithelial tumor cells acts on endothelial cells to initiate VEGF-mediated angiogenic signaling, we investigated the role of HSulf-1 in VEGF-mediated signaling using HUVECs in culture. Because HSulf-1 expression was observed in HUVECs by semiquantitative RT-PCR (Fig. 5*A*), we generated retroviral vectors expressing shRNA targeting two different regions of HSulf-1 (pSR-HSulf-1) to knock down HSulf-1 expression. Two constructs targeting different sites on HSulf-1 mRNA were mixed, packaged into viral particles, and the supernatant was used to transduce HUVECs. The empty vector (pSR alone) was used as control. After 48-hour infection, the efficacy of shRNA treatment was confirmed by the following three criteria. First, semiquantitative RT-PCR showed a marked reduction in HSulf-1 expression after

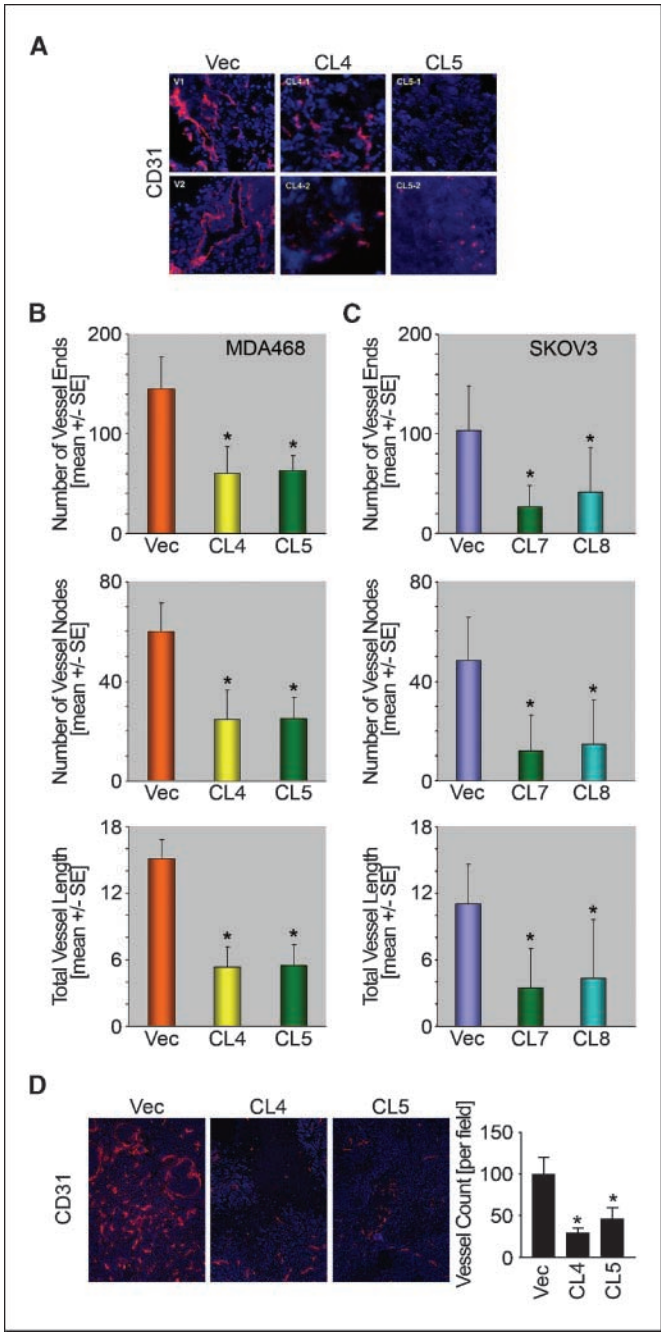

Figure 3. HSulf-1 inhibits tumor angiogenesis in nude mice. *A,* microvessel density assessment of Matrigel plugs containing MDA468 clones. MDA468 clones (10^6 cells) mixed with Matrigel were injected into nude mice and the Matrigel plugs were recovered 1 week postinjection. The plugs were sectioned and immunostained with anti-CD31 antibody (*red*) and DAPI (*blue*). Representative sections from MDA468 vector–, clone 4-, and clone 5-containing plugs. *B,* computer-generated scoring of angiogenic variables. The fluorescent micrographs were imaged at ×200 and digitally processed to generate black and white binary images for measurement of angiogenic variables (numbers of vessel ends and vessel nodes and total vessel length) using a computer-assisted scoring. About 7 to 10 random images were obtained from each Matrigel section. Vessel ends, branch points (nodes), and length were determined by an image processing tool kit (15). *C,* analyses of Matrigel plugs containing SKOV3 clones [vector-transfected or HSulf-1 stable clone 7 (*CL7*) and clone 8 (*CL8*); see ref. 12]. *, $P < 0.05$, versus vector-transfected clone. *D,* reexpression of HSulf-1 in MDA468 cells reduces blood vessel density *in vivo*. Frozen sections of MDA468 xenografts were immunolabeled with antibody to the endothelial cell marker CD31 as described. The blood vessel number was determined in digital images using NIH ImageJ software. *, $P < 0.05$, versus vector-transfected clone.

treatment with pSR-HSulf-1 compared with pSR alone (Fig. 5*A*). Second, sulfatase assay indicated that the shRNA treatment resulted in 60% suppression of sulfatase activity in HUVEC (Fig. 5*B*). Third, immunostaining using 10E4 antibody, which recognizes sulfated heparan sulfate, showed that HUVECs treated with pSR-HSulf-1 had a 3-fold increase in staining with 10E4, compared with untreated cells or cells treated with pSR alone (Fig. 5*C*). In addition, to further verify the efficacy of HSulf-1 knockdown, HEK293T cells expressing myc epitope–tagged HSulf-1 were transfected with pSR-HSulf-1 for 48 hours and the protein lysates were analyzed by Western blotting using antibody against myc epitope (Fig. 5*D*). The blot showed a striking reduction in

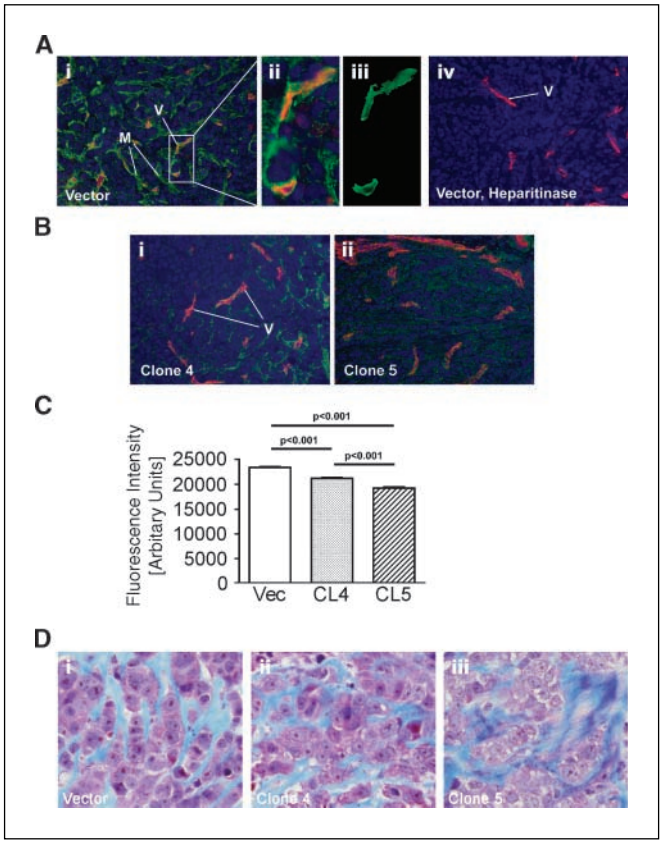

Figure 4. Glycosaminoglycan receptor complex binding assay *in situ.* The ability of tissue heparan sulfate to participate in a ternary FGF-2/FGFR1c complex was tested by measuring binding of FR1c-AP fusion protein (100 nmol/L) to frozen sections of MDA468 xenograft tumors in the presence of FGF-2 (30 nmol/L). Immobilized FR1c-AP was detected with Alexa-488-conjugated secondary antibody (*green channel*). Endothelial cells were simultaneously labeled with rat anti-CD31 antibody and visualized with Alexa-568-conjugated secondary antibody (*red channel*). DAPI served as a nuclear counterstain (*blue channel*). Sections of five tumors from each cell type were analyzed, which contained 1,276 (vector), 525 (clone 4), and 160 (clone 5) blood vessels, respectively. *A, i,* empty vector transfected control cell tumor; FR1c-AP complex is seen on tumor cell surfaces, interstitial matrix (*M*), and tumor vessels (*V*). *ii,* enlarged view of tumor vessels from (*A*); FR1c-AP complex colocalizes partially with CD31. *iii,* FR1c-AP complex signal after CD31-negative areas have been masked in Adobe Photoshop. *iv,* negative control: the tissue section (vector-transfected control tumor) was digested with heparitinase before the incubation with FGF-2 and FR1c-AP. *B,* tumor formed by HSulf-1-transfected clone 4 and 5 cells; the overall FR1c-AP binding intensity of these cells was not significantly reduced compared with vector-transfected control cells. *C,* fluorescence intensity of FR1c-AP bound in CD31-positive blood vessel areas; the vessels in clone 4 tumors bound FR1c-AP at reduced levels compared with vector-transfected tumors, and clone 5 tumors showed less binding than clone 4 tumors ($P < 0.001$ for both). *D,* the tumor xenografts were stained with Masson's trichrome stain, which colors collagen blue and nuclei and cytoplasm red. Original magnification, ×400 (except *Aii* and *Aiii*).

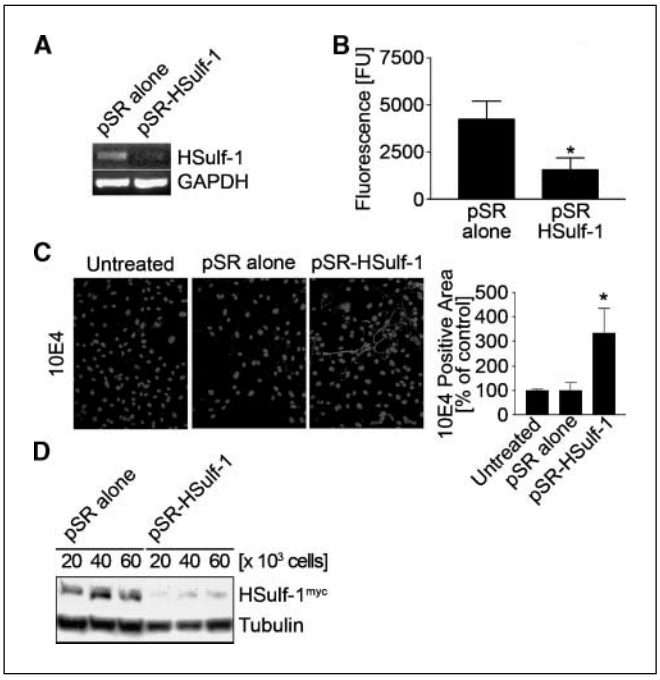

Figure 5. Down-regulation of HSulf-1 in HUVEC by retroviral expression of shRNA. HUVECs were transduced with retrovirus containing pSR-HSulf-1 or pSR alone for 48 hours and the down-regulation of HSulf-1 confirmed by the following criteria: RT-PCR (*A*), sulfatase activity (*B*; *, $P < 0.05$, versus vector-transfected control), and immunostaining for 10E4 epitope (*C*; *red*), which recognizes native heparan sulfate with sulfated glucosamine residues (12). The samples stained with 10E4 were costained with DAPI (*blue*) to identify the nuclei. Images were taken with 20× objective. *C, right,* quantification of the 10E4-positive area by image analysis. Three different fields in each sample were analyzed. *, $P < 0.05$, versus vector-transfected control. *D,* down-regulation of HSulf-1-myc protein expressed in 293T cells by pSR-HSulf-1. Cells transfected with plasmid vector expressing HSulf-1-myc on the day before were plated at different densities in 24-well plates and then transduced with pSR-HSulf-1 or pSR alone for 48 hours. The HSulf-1-myc protein was detected by Western blot using anti-myc antibody.

HSulf-1-myc protein level achieved by the pSR-HSulf-1 treatment compared with pSR alone. These data show a significant down-regulation in HSulf-1 expression achieved by the HSulf-1 shRNA retroviral transfection.

HUVEC with down-regulated HSulf-1 showed increased $VEGF_{165}$-mediated cell proliferation. During angiogenesis, endothelial cells proliferate and migrate to sprout from preexisting vessels (1). To see if HSulf-1 knockdown could modulate endothelial cell proliferation, HUVECs treated with pSR-HSulf-1 or pSR alone were stimulated with various growth factors in the presence of [^{3}H]thymidine for 24 hours and the incorporated radioactivity was quantified (Fig. 6*A*). The cells treated with pSR-HSulf-1 showed significantly higher degree of [^{3}H]thymidine incorporation when stimulated with heparin-binding angiogenic factors, such as $VEGF_{165}$, FGF-2, and hepatocyte growth factor, compared with the cells treated with pSR alone. In contrast, only a minor difference in [^{3}H]thymidine incorporation was observed between cells treated with pSR-HSulf-1 and pSR alone when proliferation was stimulated by $VEGF_{121}$, an isoform lacking the heparin-binding domain. In addition, when HUVECs were treated with pSR-HSulf-1 together with sodium chlorate, a metabolic inhibitor of HSPG sulfation, the level of [^{3}H]thymidine incorporation stimulated with $VEGF_{165}$ was comparable to that of vector-treated cells. These data indicate that HSulf-1 knockdown increases

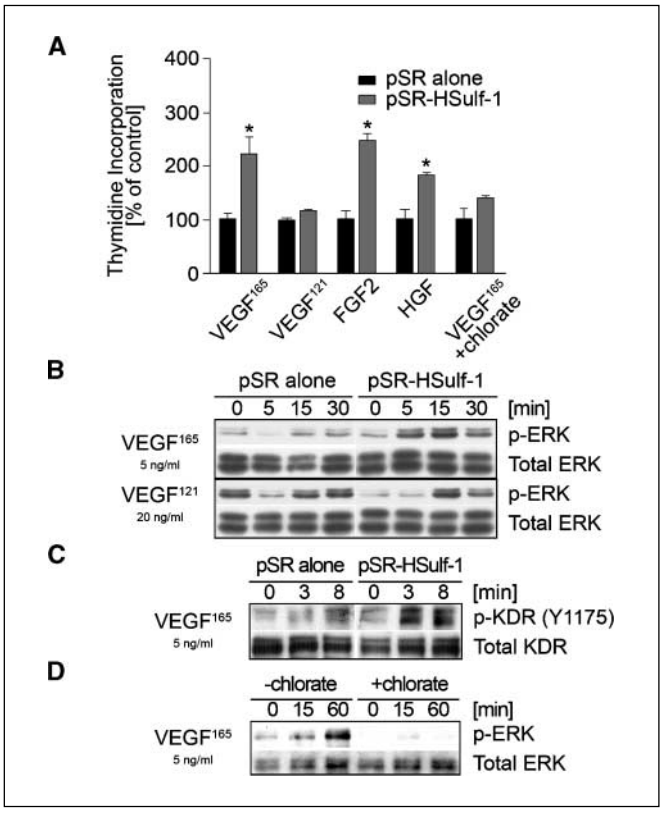

Figure 6. Down-regulation of HSulf-1 in HUVEC causes increased cell proliferation in response to heparin-binding growth factors. *A,* HSulf-1 down-regulation enhances HUVEC proliferation stimulated by heparin-binding growth factors. Cells infected with pSR-HSulf-1 or pSR alone were stimulated with various growth factors for 24 hours in the presence of [^{3}H]thymidine. The amounts of radioactivity incorporated in a trichloroacetic acid–precipitated fraction were counted. Results were expressed as fold increase compared with control HUVEC infected with pSR alone. *, $P < 0.05$, versus vector-transfected control. *B* and *C,* HSulf-1 down-regulation potentiates $VEGF_{165}$-mediated signaling in HUVEC. Cells transduced with pSR-HSulf-1 or pSR alone were serum starved overnight and stimulated with VEGF isoforms as indicated. Whole-cell lysates were subjected to SDS-PAGE, transferred to PVDF, and sequentially probed with antibodies for phospho-/total ERK1/2 (*B*) or phospho-/total KDR (*C*). *D,* desulfation of HSPGs in HUVECs by chlorate treatment inhibits $VEGF_{165}$ signaling. HUVEC cells were cultured in sulfate-free medium with or without 15 mmol/L sodium chlorate for 48 hours, serum starved overnight, and stimulated with 5 ng/mL VEGF for 15 and 60 minutes. Whole-cell lysates were subjected to SDS-PAGE, transferred to PVDF, and sequentially probed with phosphorylated ERK1/2 and total ERK1/2.

HUVEC cell proliferation mediated by heparan sulfate–binding (but not heparan sulfate–independent) growth factors.

Based on previous reports that increased proliferation caused by VEGF correlates with ERK activation (12–14), we analyzed ERK activation in HUVECs following shRNA-mediated HSulf-1 down-regulation. The transfected cells were serum starved overnight, stimulated with various growth factors, and the degree of ERK1/2 activation was analyzed by Western blot using phosphospecific antibody against ERK1/2 (Fig. 6*B*). Consistent with the [^{3}H]thymidine incorporation assay, the shRNA-treated cells showed a higher degree of ERK1/2 phosphorylation at 5 and 15 minutes following $VEGF_{165}$ stimulation. On the other hand, vector-treated cells showed only modest increases in ERK1/2 phosphorylation under the same conditions. By contrast, no major differences in ERK1/2 phosphorylation were observed between cells treated with pSR-HSulf-1 and cells treated with pSR alone when stimulated with heparin-independent $VEGF_{121}$ (Fig. 6*B*). To see if the increase in ERK phosphorylation was due to the enhanced activation of VEGF receptor, KDR, the degree of KDR phosphorylation was also analyzed (Fig. 6*C*). The Western blot indicated that the cells treated with pSR-HSulf-1 showed a higher degree of KDR phosphorylation immediately after stimulation (3 and 8 minutes) with $VEGF_{165}$, indicating that HSulf-1 knockdown and the resulting hypersulfation of HSPGs enhance the activity of $VEGF_{165}$. The importance of HSPG sulfation in $VEGF_{165}$ signaling was further shown by treating the cells with sodium chlorate, a metabolic inhibitor of HSPG sulfation. Pretreatment of HUVECs with 15 mmol/L chlorate for 48 hours abolished $VEGF_{165}$-mediated phosphorylation of ERK1/2 (Fig. 6*D*). Taken together, these data show that down-regulation of HSulf-1 in HUVEC results in increased levels of HSPG sulfation and higher degree of cell proliferation in response to $VEGF_{165}$, supporting the regulatory role of HSulf-1 in VEGF-mediated proliferation.

Discussion

The goal of the present work was to evaluate the role of HSulf-1 in modulating tumorigenesis and angiogenesis *in vitro* and *in vivo*. To study the role of HSulf-1 in tumorigenesis *in vitro*, stable clones of MDA468 breast cancer cells expressing HSulf-1 were generated, and cell growth was monitored by direct counting with a hemocytometer (Fig. 1). These results show that HSulf-1 expression reduces the growth rate of breast cancer cells, consistent with previous reports indicating that HSulf-1 expression attenuates heparin-binding growth factor signaling leading to reduced growth rate of several cancer cell lines (12–14). To investigate the effect of HSulf-1 expression *in vivo*, stable clones of MDA468 breast cancer cells expressing HSulf-1 were injected in mice and the tumor growth was monitored. HSulf-1 clonal lines exhibited a significant reduction in tumor volume compared with the vector-transfected clone (Fig. 2*A*), similar to what was observed by Dai et al. (22) in myeloma model. Moreover, xenografts derived from HSulf-1–expressing cells were avascular and showed marked necrosis and apoptosis compared with xenografts derived from the vector-transfected MDA468 clone (Fig. 2*B* and *C*). This suggests that the injected cells might be exposed to a poor supply of nutrients and oxygen, which restricts tumor growth, in agreement with a generally accepted concept that the growth of solid tumors is dependent on their ability to induce tumor angiogenesis (23). Indeed, immunostaining of the Matrigel sections for an endothelial marker, CD31, revealed a dramatic decrease in tumor microvessel formation in HSulf-1 clones (Fig. 3*A* and *B*). The inhibition of tumor angiogenesis by HSulf-1 was also observed in ovarian cancer cell line Matrigel plugs (Fig. 3*C*), indicating that these observations were not limited to the tumor model chosen. Similar to our observation, heparin treated with QSulf-1, a quail homologue of HSulf-1, inhibited angiogenesis in chicken chorioallantoic membrane assay (24). Furthermore, knockdown of a heparan sulfate 6-*O* sulfotransferase (HS6ST2) in zebrafish resulted in abnormalities in the branching morphogenesis of the caudal vein during embryogenesis (25).

An important difference between this work and the findings reported by Dai et al. (22) is the fact that in breast carcinomas, HSulf expression leads to reduced vessel density whereas no such effect was seen in the myeloma. The differences could be due to the types of tumors analyzed, as solid tumors such as breast and ovarian cancers are more angiogenic dependent compared with myeloma. In addition, HSulf-1 expression in the myeloma cells leads to the accumulation of abundant pericellular matrix material, which may have sequestered the enzyme. In contrast, trichrome stains show

that in MDA468 mammary carcinoma cells, HSulf-1 expression is not associated with a recognizable increase in extracellular matrix (Fig. 4*D*), further reiterating the differences between the two tumor types. Our glycosaminoglycan receptor complex binding assay data indicate that vascular heparan sulfate in HSulf-1-positive mammary carcinomas has a significantly reduced ability to support a stable complex with FGF-2 and FGFR1c (Fig. 4*A-C*). Down-regulation of HSulf-1 in tumor cells could increase 6-*O* sulfated HSPGs in the tumor microenvironment shared by both tumor and endothelial cells, leading to enhanced angiogenesis. To check whether HSulf expression resulted in diminished production of proangiogenic factors, we determined VEGF and basic FGF (bFGF) levels by ELISA. There was no significant change in the levels of VEGF or bFGF in the conditioned media or the cell lysates of HSulf-1 clonal lines compared with the vector-transfected MDA468 clones as determined by ELISA (data not shown). Irrespective of this, the presence of HSulf-1 in tumors could modulate VEGF-mediated signaling without altering VEGF levels (10). Based on these observations, we conclude that changes in HSPG sulfation by HSulf-1, leading to the 6-*O* desulfation, may inhibit tumor angiogenesis *in vivo*.

Dai et al. (22) have shown that both HSulf-1 and HSulf-2 are potent inhibitors of growth *in vivo*. Whether HSulf-2 has a similar phenotype in breast and ovarian tumors is currently unknown. Interestingly, a recent report by Morimoto et al. (26) implicates Sulf-2 as a promoter of angiogenesis in breast cancer. This is in contrast to this study where we have clearly shown HSulf-1 ability to inhibit angiogenesis. Because breast tumor growth is angiogenic dependent, whether or not HSulf-2 will inhibit tumor growth *in vivo* is currently unknown.

The knockdown of HSulf-1 expression in HUVECs by shRNAs potentiated the activity of various heparin-binding growth factors to increase cell proliferation (Fig. 5*A*). Because of the significant importance of VEGF in tumor angiogenesis (27), the effect of HSulf-1 on VEGF signaling was investigated in detail. As expected, HUVECs with HSulf-1 knockdown showed enhanced phosphorylation of KDR and ERK1/2 in response to the heparin-binding $VEGF_{165}$, but not heparin-independent $VEGF_{121}$ (Fig. 5*B*). This is consistent with a study using various chemically modified heparins showing the requirement of 6-*O* sulfate group for interaction with $VEGF_{165}$ (10). The enhancement in KDR phosphorylation at Tyr^{1175}, which is known to be essential for VEGF-dependent MAPK activation and proliferation (28), is also in agreement with a previous report that highly sulfated HSPGs potentiate interaction between VEGF and KDR (8). Taken together, these data show the potential regulatory role of HSulf-1 in the angiogenic response of HUVECs.

Angiogenesis is regulated by the balance between a variety of angiogenic and antiangiogenic factors (1). The fact that considerable numbers of these factors interact with heparan sulfate to enhance or inhibit its activities implies a potential regulatory role of HSulf-1 in this complex biological event. One of the steps in the malignant progression of cancer cells is an angiogenic switch from a nonangiogenic phenotype. The angiogenic switch involves a cascade of biological effects on the endothelium. This includes, but is not restricted to, overexpression of oncogenes and down-regulation of novel tumor suppressor genes, and secretion of a number of growth factors that may act by paracrine and autocrine pathways (29). Angiogenesis is critical for primary tumor growth because beyond a critical volume, a tumor cannot expand further without neovascularization. Intratumor microvessel density is a measure of the extent of new blood vessel formation and a surrogate marker of the degree of angiogenesis in breast cancer. Several reports have shown a direct correlation of increases in microvessel density to poor prognosis, worse disease-free survival, and overall survival by univariate analysis (30). Whether HSulf-1 is one of the markers of this angiogenic switch is currently under investigation.

Overexpression of VEGF by ovarian cancer cells is obligatory for ascites formation (31). Inhibiting VEGF-mediated signaling with a neutralizing antibody (A4.6.1) to VEGF resulted in reduction in ascites and reduced i.p. tumor growth in an *in vivo* mouse model (32). We previously reported that >75% of primary ovarian tumors lack HSulf-1 expression. We have previously shown that the presence of HSulf-1 in cancer cells sensitizes these cells to commonly used chemotherapeutic agents such as cisplatin and taxol (12–14). Resistance to chemotherapy is a common problem encountered in ovarian and other solid tumors. However, a combination therapy that combines inhibition of angiogenesis with traditional chemotherapeutic agents may have an additive effect of inhibiting tumor growth and metastases *in vivo* (33–35). Given the observation that the presence of HSulf-1 inhibits angiogenesis *in vivo*, it is anticipated that the chemotherapeutic effect would be beneficial *in vivo* for cells with HSulf-1 expression. This highly innovative approach of using the knowledge of the genetic background to determine which of the patients may benefit from aggressive chemotherapy may lead to customized therapies in women whose tumors no longer express HSulf-1.

Our finding that expression of HSulf-1 in cancer cells inhibits tumorigenesis and tumor angiogenesis suggests that the modification of HSPG polysaccharide structure could be a reasonable approach for the treatment of cancer, in addition to or in combination with conventional chemotherapy and antiangiogenic therapy. Indeed, low molecular weight heparin-mimicking derivatives of 5K polysaccharide from *Escherichia coli* have been shown to have antiangiogenic activity (36). It will be of interest to test if HSulf-1–treated heparins, or HSulf-1 protein itself, will have a similar antiangiogenic activity and if the expression of HSulf-1 in tumors can predict clinical outcome in patients with cancer.

Acknowledgments

Received 10/5/2005; revised 4/5/2006; accepted 4/12/2006.

Grant support: National Cancer Institute grant CA106954-01 (V. Shridhar). Minnesota Ovarian Cancer Alliance (V. Shridhar). John W. Anderson Foundation (V. Shridhar), and Mayo Foundation (V. Shridhar).

The costs of publication of this article were defrayed in part by the payment of page charges. This article must therefore be hereby marked *advertisement* in accordance with 18 U.S.C. Section 1734 solely to indicate this fact.

We thank Kimberely Kalli for critical reading of the manuscript and Mark Schroeder and David James for their help with the xenografts.

References

1. Carmeliet P, Jain RK. Angiogenesis in cancer and other diseases. Nature 2000;407:249–57.
2. Kerbel R, Folkman J. Clinical translation of angiogenesis inhibitors. Nat Rev Cancer 2002;2:727–39.
3. Ferrara N. Vascular endothelial growth factor. Eur J Cancer 1996;32A:2413–22.
4. Weidner N, Semple JP, Welch WR, Folkman J. Tumor angiogenesis and metastasis-correlation in invasive breast carcinoma. N Engl J Med 1991;324:1–8.
5. Macchiarini P, Fontanini G, Hardin MJ, Squartini F, Angeletti CA. Relation of neovascularisation to metastasis of non-small-cell lung cancer. Lancet 1992;340:145–6.
6. Weidner N, Carroll PR, Flax J, Blumenfeld W, Folkman J. Tumor angiogenesis correlates with metastasis in invasive prostate carcinoma. Am J Pathol 1993;143:401–9.

7. Paley PJ, Staskus KA, Gebhard K, et al. Vascular endothelial growth factor expression in early stage ovarian carcinoma. Cancer 1997;80:98–106.
8. Soker S, Goldstaub D, Svahn CM, Vlodavsky I, Levi BZ, Neufeld G. Variations in the size and sulfation of heparin modulate the effect of heparin on the binding of VEGF165 to its receptors. Biochem Biophys Res Commun 1994;203:1339–47.
9. Tessler S, Rockwell P, Hicklin D, et al. Heparin modulates the interaction of VEGF165 with soluble and cell associated flk-1 receptors. J Biol Chem 1994;269: 12456–61.
10. Ono K, Hattori H, Takeshita S, Kurita A, Ishihara M. Structural features in heparin that interact with VEGF165 and modulate its biological activity. Glycobiology 1999;9:705–11.
11. Lundin L, Larsson H, Kreuger J, et al. Selectively desulfated heparin inhibits fibroblast growth factor-induced mitogenicity and angiogenesis. J Biol Chem 2000;275:24653–60.
12. Lai J, Chien J, Staub J, et al. Loss of HSulf-1 up-regulates heparin-binding growth factor signaling in cancer. J Biol Chem 2003;278:23107–17.
13. Lai JP, Chien JR, Moser DR, et al. hSulf1 Sulfatase promotes apoptosis of hepatocellular cancer cells by decreasing heparin-binding growth factor signaling. Gastroenterology 2004;126:231–48.
14. Lai JP, Chien J, Strome SE, et al. HSulf-1 modulates HGF-mediated tumor cell invasion and signaling in head and neck squamous carcinoma. Oncogene 2004;23: 1439–47.
15. Wild R, Ramakrishnan S, Sedgewick J, Griffioen AW. Quantitative assessment of angiogenesis and tumor vessel architecture by computer-assisted digital image analysis: effects of VEGF-toxin conjugate on tumor microvessel density. Microvasc Res 2000;59:368–76.
16. Chang Z, Meyer K, Rapraeger AC, Friedl A. Differential ability of heparan sulfate proteoglycans to assemble the fibroblast growth factor receptor complex *in situ*. FASEB J 2000;14:137–44.
17. Friedl A, Filla M, Rapraeger AC. Tissue-specific binding by FGF and FGF receptors to endogenous heparan sulfates. Methods Mol Biol 2001;171:535–46.
18. Berns K, Hijmans EM, Mullenders J, et al. A large-scale RNAi screen in human cells identifies new components of the p53 pathway. Nature 2004;428:431–7.
19. Clayton A, Thomas J, Thomas GJ, Davies M, Steadman R. Cell surface heparan sulfate proteoglycans control the response of renal interstitial fibroblasts to fibroblast growth factor-2. Kidney Int 2001;59:2084–94.
20. Chien J, Shah GV. Role of stimulatory guanine nucleotide binding protein (GSα) in proliferation of PC-3M prostate cancer cells. Int J Cancer 2001;91:46–54.
21. Folkman J. Angiogenesis in cancer, vascular, rheumatoid and other disease. Nat Med 1995;1:27–31.
22. Dai Y, Yang Y, Macleod V, et al. HSulf-1 and HSulf-2 are potent inhibitors of myeloma tumor growth *in vivo*. J Biol Chem 2005;280:40066–73.
23. Neri D, Bicknell R. Tumour vascular targeting. Nat Rev Cancer 2005;5:436–46.
24. Wang S, Ai X, Freeman SD, et al. QSulf1, a heparan sulfate 6-O-endosulfatase, inhibits fibroblast growth factor signaling in mesoderm induction and angiogenesis. Proc Natl Acad Sci U S A 2004;101:4833–8.
25. Chen E, Stringer SE, Rusch MA, Selleck SB, Ekker SC. A unique role for 6-O sulfation modification in zebrafish vascular development. Dev Biol 2005;284:364–76.
26. Morimoto-Tomita M, Uchimura K, Bistrup A, et al. Sulf-2, a proangiogenic heparan sulfate endosulfatase, is up-regulated in breast cancer. Neoplasia 2005;7:1001–10.
27. Ferrara N, Hillan KJ, Novotny W. Bevacizumab (Avastin), a humanized anti-VEGF monoclonal antibody for cancer therapy. Biochem Biophys Res Commun 2005; 333:328–35.
28. Sakurai Y, Ohgimoto K, Kataoka Y, Yoshida N, Shibuya M. Essential role of Flk-1 (VEGF receptor 2) tyrosine residue 1173 in vasculogenesis in mice. Proc Natl Acad Sci U S A 2005;102:1076–81.
29. Folkman J. Role of angiogenesis in tumor growth and metastasis. Semin Oncol 2002;29:15–8.
30. Guidi AJ, Berry DA, Broadwater G, et al. Association of angiogenesis and disease outcome in node-positive breast cancer patients treated with adjuvant cyclophosphamide, doxorubicin, and fluorouracil: a Cancer and Leukemia Group B correlative science study from protocols 8541/8869. J Clin Oncol 2002;20: 732–42.
31. Folkman J. A new link in ovarian cancer angiogenesis: lysophosphatidic acid and vascular endothelial growth factor expression. J Natl Cancer Inst 2001; 93:734–5.
32. Mesiano S, Ferrara N, Jaffe RB. Role of vascular endothelial growth factor in ovarian cancer: inhibition of ascites formation by immunoneutralization. Am J Pathol 1998;153:1249–56.
33. Borgstrom P, Gold DP, Hillan KJ, Ferrara N. Importance of VEGF for breast cancer angiogenesis *in vivo*: implications from intravital microscopy of combination treatments with an anti-VEGF neutralizing monoclonal antibody and doxorubicin. Anticancer Res 1999;19: 4203–14.
34. Hu L, Hofmann J, Zaloudek C, Ferrara N, Hamilton T, Jaffe RB. Vascular endothelial growth factor immunoneutralization plus Paclitaxel markedly reduces tumor burden and ascites in athymic mouse model of ovarian cancer. Am J Pathol 2002;161:1917–24.
35. Soffer SZ, Moore JT, Kim E, et al. Combination antiangiogenic therapy: increased efficacy in a murine model of Wilms tumor. J Pediatr Surg 2001;36:1177–81.
36. Presta M, Oreste P, Zoppetti G, et al. Antiangiogenic activity of semisynthetic biotechnological heparins: low-molecular-weight-sulfated *Escherichia coli* K5 polysaccharide derivatives as fibroblast growth factor antagonists. Arterioscler Thromb Vasc Biol 2005;25:71–6.